McMillan-Ginzburg-Landau theory of singularities and discommensurations in charge density wave states of transition metal dichalcogenides

V. N. Moura,[1] A. Chaves,[1,2,*] F. M. Peeters,[1,2] and M. V. Milošević[2,3,†]

[1]*Departamento de Física, Universidade Federal do Ceará, Caixa Postal 6030, Campus do Pici, 60455-900 Fortaleza, Ceará, Brazil*

[2]*Department of Physics, University of Antwerp, Groenenborgerlaan 171, B-2020 Antwerp, Belgium*

[3]*Instituto de Física, Universidade Federal de Mato Grosso, Cuiabá, Mato Grosso 78060-900, Brazil*

(Received 7 December 2023; revised 21 February 2024; accepted 22 February 2024; published 11 March 2024)

The McMillan-Ginzburg-Landau (MGL) model for charge density waves (CDW) is employed in a systematic phenomenological study of the different phases that have been probed in recent experiments involving transition metal dichalcogenides. We implemented an efficient imaginary time evolution method to solve the MGL equations, which enabled us to investigate the role of different coupling parameters on the CDW patterns and to perform calculations with different energy functionals that lead to several experimentally observed singularities in the CDW phase profiles. In particular, by choosing the appropriate energy functionals, we were able to obtain phases that go beyond the well-known periodic phase slips (discommensurations), exhibiting also topological defects (i.e., vortex-antivortex pairs), domain walls where the CDW order parameter is suppressed, and even CDW with broken rotational symmetry. Finally, we briefly discuss the effect of these different CDW phases on the profile and critical temperature of the competing superconducting state.

DOI: 10.1103/PhysRevB.109.094507

I. INTRODUCTION

The competition between different collective phases and their interplay are of pertinent interest in solid-state physics. For example, the iron-based materials can exhibit high-temperature superconductivity in competition with other collective phenomena, such as nematic order [1–3], antiferromagnetism [4], and charge/spin density waves [5]. In recent studies, atomically thin transition-metal dichalcogenides (TMDs) have shown emergent superconductivity when doped [6,7], exhibiting a dome of superconducting (SC) phase in the low-temperature region of the temperature versus doping phase diagram. It has been suggested that the fluctuations of their charge density wave (CDW) order, possibly in the form of discommensurations (DC), are closely related to effectively enhancing the superconducting critical temperature [8–11]. It is therefore of fundamental importance to develop theoretical models that allow one to capture and understand the interplay between the SC and CDW order parameters and provide predictive power about the phase diagram of these materials.

Using a technique based on scanning tunneling microscopy (STM), Pasztor *et al.* [12] were able to retrieve images with high spatial resolution of the CDW phase in VSe_2 and $NbSe_2$. This technique enables one to separately obtain amplitude and phase maps of the different order parameters that compose the CDW profile. Their analysis provides evidence that the charge density wave of these TMDs consists of three individual charge modulation order parameters. Moreover, phase images revealed not only discommensurations in the nearly commensurate state, which have been predicted by McMillan theory [10], but also topological defects and domain walls.

Recently, a McMillan-Ginzburg-Landau model (MGL) [9] was used to describe the pathway from incommensurate to commensurate CDW phases in the phase diagram of TMDs, where the discommensurations in the near-commensurate phase were observed. A coupling between the CDW and SC phases was then suggested in the form of a modulation of the quadratic term on the SC order parameter, within the Ginzburg-Landau energy functional, that is proportional to the gradient of the CDW order parameter. With this approach, the SC dome in the near-commensurate region of the phase diagram of the TMD could be phenomenologically modelled, as the SC phase emerges in regions with high variation of the CDW order parameters, such as in the discommensurations. Similar ways of coupling the SC, CDW and spin density wave (SDW) phases have also been proposed in previous theoretical works [13,14]. However, prediction and control of the profile of the SC dome in the phase diagram of different TMD-based systems requires a deeper analysis of the role of different parameters in the MGL model, as well as on the effect of the experimentally observed phase domain walls and topological defects in the CDW spatial configuration.

In this paper, we analyze the effect of different parameters in the MGL functional on the phase distribution, discommensurations, singularities, and critical temperatures of CDW and SC phases in transition metal dichalcogenides. We employ an imaginary time evolution method [15] to obtain the lowest energy solution for the MGL equations in an efficient manner. We demonstrate that a proper choice of phenomenological parameters in the MGL energy functional allows one to obtain not only the well-known CDW discommensuration, but

*andrey@fisica.ufc.br

†milorad.milosevic@uantwerpen.be

also topological defects, such as vortex-antivortex pairs, phase domain walls where the CDW order parameter is locally suppressed, and even the unidirectional CDW profiles in systems where C_{6v} symmetry is expected otherwise. Finally, we also use the CDW profile as an input for a calculation of the critical temperature of a competing SC order parameter, which emerges in regions where CDW is suppressed. Our results help to unravel the mechanism behind the formation of the SC dome in the temperature versus doping phase diagram of these systems, thus allowing us to propose situations where the width and maximum critical temperature of such a dome can be enhanced.

The paper is organized as follows. Section II details the theoretical formalism and our numerical approach to solving the McMillan-Ginzburg-Landau equations. The results are presented in Sec. III, where different subsections are devoted to the discussion of different CDW features of interest, and finally the superconducting phase as well. Section IV summarizes our conclusions.

II. THEORETICAL FRAMEWORK

A. Energy functionals

The transition between commensurate and incommensurate states was phenomenologically described in the seminal work of McMillan [10] in terms of a free-energy functional with complex order parameters, much like the GL theory for superconductivity. Within this framework, we use an extension of the McMillan functional to account for the symmetries of transition metal dichalcogenides, such as $TaSe_2$, VSe_2, and $NbSe_2$, where such CDW phases were recently observed [12,16–18]. We start from the density modulation of commensurate CDW [9],

$$\rho(\mathbf{r}) = \sum_j e^{i\mathbf{r}\cdot\mathbf{Q}_j^C}\psi_j + \text{c.c.}, \tag{1}$$

where ψ_j is the order parameter associated with the commensurate wave-vector in the j-th direction $\mathbf{Q}_j^C$, given as integer, or half-integer, multiples of the primitive reciprocal vectors $\mathbf{G}_j$ of the material. In the case of the transition metal dichalcogenides investigated here, there are three of such primitive reciprocal vectors ($j = 1$, 2, or 3), rotated 120° with respect to each other.

The complex order parameters can be rewritten in terms of their amplitude $\phi_j(\mathbf{r})$ and phase $\theta_j(\mathbf{r})$ as $\psi_j(\mathbf{r}) = \phi_j(\mathbf{r})\exp[i\theta_j(\mathbf{r})]$, where the phase parameter quantifies the deviations in comparison to the commensurate wave-vector. For instance, the incommensurate CDW phase in the jth direction is characterized by $\theta_j(\mathbf{r}) = \mathbf{q}_j^I \cdot \mathbf{r}$, where the incommensurability vector $\mathbf{q}_j^I \equiv \delta_j \mathbf{Q}_j^C$ leads to an effective wave-vector $\mathbf{Q}_j^C(1+\delta_j)$ in Eq. (1) so that the δ_j parameter quantifies the deviation from the otherwise commensurate lattice in that direction.

The MGL energy functional for TMDs carries the contribution of the three order parameters ψ_j that generate the CDW, the energy of the superconducting phase, characterized by the order parameter Φ, along with a coupling term between superconductivity and the CDW, characterized by the coupling parameter γ [1,4,13,14], i.e.,

$$f = f_0 + f_1 + f_s + \gamma\sum_j |\psi_j|^2|\Phi|^2, \tag{2}$$

where the McMillan functional $f_M = f_0 + f_1$ is composed of [10,19]

$$f_0 = \sum_j \left[\alpha\tau|\psi_j|^2 + G|\psi_j|^4 + B\left|\left(i\nabla + \mathbf{q}_j^I\right)\psi_j\right|^2\right], \tag{3}$$

with the effective temperature parameter $\tau = T/T_{\text{cdw}} - 1$, and

$$f_1 = -\frac{E}{2}\sum_j\left(\psi_j^2 + \psi_j^{*2}\right) - \frac{3D}{2}(\psi_1\psi_2\psi_3 + \text{c.c.}) + \frac{K}{2}\sum_{i,j>i}|\psi_i\psi_j|^2 - \frac{M}{2}\sum_{j,k\neq l\neq j}(\psi_j\psi_k^*\psi_l^* + \text{c.c.}). \tag{4}$$

While the Ginzburg-Landau-like energy functional f_0 accounts simply for a phase transition from normal to CDW phases at $T = T_{\text{cdw}}$, the f_1 functional accounts for the couplings between different order parameters, as well as for the energy dependence on the total charge density, via the lock-in energy E, [10] which is characteristic of McMillan theory of CDW.

In such a phenomenological energy functional, different coupling terms between order parameters and their gradients are possible. However, the resulting CDW built with the ψ_j order parameters as in Eq. (1) must obey certain material-dependent symmetry properties, which eventually reflects on the choice of coupling terms. To the lowest order in ψ_j, the C_{3v}, mirror, and inversion symmetries of the CDW in transition metal dichalcogenides allow for the coupling terms presented in f_1. For detailed information on these coupling terms and phenomenological coefficients in Eq. (4), we refer to the Supplemental Material of Ref. [9].

The superconductor energy density f_s is given by

$$f_s = \alpha_s|\Phi|^2 + \frac{\beta}{2}|\Phi|^4 + \frac{1}{4m}\left|\frac{\hbar}{i}\nabla\Phi\right|^2, \tag{5}$$

where the phenomenological coefficients are the same as in the usual GL theory of superconductivity. The biquadratic term we use for coupling CDW profiles and SC, i.e., $\gamma\sum_j|\psi_j|^2|\Phi|^2$ in Eq. (2), is discussed in detail in Ref. [13].

From f_0, it becomes clear that the B term favors the incommensurate solution, by yielding lower energy as $\theta_j(\mathbf{r})$ approaches $\mathbf{q}_j^I \cdot \mathbf{r}$. However, the $E > 0$ term in f_1 favors the commensurate solution: since $(\psi_j^2 + \psi_j^{*2}) = 2\phi_j^2\cos(2\theta_j)$, the energy is minimized as the phase approaches $\theta_j \equiv n\pi$, for integer n.

Better physical insight is obtained by using an effective mass term m^* to rewrite $B = \hbar^2/2m^*$. Three Euler-Lagrange equations, one for each j direction, are derived from the minimization of the McMillan functional:

$$\left[\alpha\tau + G|\psi_j|^2 + \frac{K}{2}(|\psi_l|^2 + |\psi_k|^2) + \gamma|\Phi|^2\right]\psi_j - E\psi_j^* - \frac{\hbar^2}{2m^*}\left(i\nabla + \mathbf{q}_j^I\right)^2\psi_j + \frac{3D}{2}(\psi_l^*\psi_k^*) - \frac{M}{2}(\psi_l\psi_k + 2\mathbb{R}[\psi_l\psi_k]) = 0, \tag{6}$$

where $l \neq k \neq j$ and $l \neq j$. We define a characteristic length $\xi = \sqrt{\hbar^2/2m^*\alpha}$ and rescale energies by α. Equation (6) thus becomes

$$\left[\tau + \frac{G}{\alpha}|\psi_j|^2 + \frac{K}{2\alpha}(|\psi_l|^2 + |\psi_k|^2) + \frac{\gamma}{\alpha}|\Phi|^2\right]\psi_j - \frac{E}{\alpha}\psi_j^* - \xi^2\left(i\nabla + \mathbf{q}_j^I\right)^2\psi_j + \frac{3D}{2\alpha}(\psi_l^*\psi_k^*) - \frac{M}{2\alpha}(\psi_l\psi_k + 2\mathbb{R}[\psi_l\psi_k]) = 0. \quad (7)$$

For the superconducting order parameter, the Euler-Lagrange equation that minimizes f_s is simply the GL equation, coupled to the CDW parameter by γ [13]:

$$(\alpha_s + \beta|\Phi|^2)\Phi - \frac{1}{4m}\left(\frac{\hbar}{i}\nabla\right)^2\Phi + \gamma\Phi\sum_j|\psi_j|^2 = 0. \quad (8)$$

B. Time evolution technique

The set of coupled Eqs. (7) and (8) is solved by evolving a set of arbitrary initial wavefunctions $\psi_j(x, y, t = 0)$ and $\Phi(x, y, t = 0)$ in time until convergence is reached, a technique that has been successfully employed, e.g., in the mathematically similar case of Gross-Pitaevskii equations (GPe) in the context of Bose-Einstein condensation [20–23].

The time evolution of McMillan-Ginzburg-Landau equations reads

$$\left[\tau + \frac{G}{\alpha}|\psi_j|^2 + \frac{K}{2\alpha}(|\psi_l|^2 + |\psi_k|^2) + \frac{\gamma}{\alpha}|\Phi|^2\right]\psi_j - \frac{E}{\alpha}\psi_j^* - \xi^2\left(i\nabla + \mathbf{q}_j^I\right)^2\psi_j + \frac{3D}{2\alpha}(\psi_l^*\psi_k^*) - \frac{M}{2\alpha}(\psi_l\psi_k + 2\mathbb{R}[\psi_l\psi_k]) = \Gamma_M\frac{\partial\psi_j}{\partial t};$$
$$(\alpha_s + \beta|\Phi|^2)\Phi - \frac{1}{4m}\left(\frac{\hbar}{i}\nabla\right)^2\Phi + \gamma\Phi\sum_j|\psi_j|^2 = \Gamma_{\mathrm{GL}}\frac{\partial\Phi}{\partial t}, \quad (9)$$

where $\Gamma_{M(\mathrm{GL})}$ are damping parameters. The ψ_j and Φ functions that solve Eqs. (7) and (8) are the stationary solutions of Eq. (9). The case of GPe differs only by the fact that the time derivative is multiplied by $i = \sqrt{-1}$, so that the evolution that leads to stationary functions in GPe must be performed in imaginary time it, while in the case of MGL equations, this is done in real time.

We rewrite Eq. (9) as

$$\hat{F}_M\psi_j = [\hat{T}_M + \hat{V}_M(|\psi_j|^2)]\psi_j = \Gamma_M\frac{\partial\psi_j}{\partial t},$$
$$\hat{F}_{\mathrm{GL}}\Phi = [\hat{T}_{\mathrm{GL}} + \hat{V}_{\mathrm{GL}}(|\Phi|^2)]\Phi = \Gamma_{\mathrm{GL}}\frac{\partial\Phi}{\partial t}, \quad (10)$$

by defining the operators

$$\hat{V}_M(|\psi_j|^2) = \left[\tau + \bar{G}|\psi_j|^2 + \frac{\bar{K}}{2}(|\psi_l|^2 + |\psi_k|^2) + \bar{\gamma}|\Phi|^2\right] - \bar{E}\frac{\psi_j^*}{\psi_j} + \frac{3\bar{D}}{2\psi_j}(\psi_l^*\psi_k^*) - \frac{\bar{M}}{2\psi_j}(\psi_l\psi_k + 2\mathbb{R}[\psi_l\psi_k]),$$
$$\hat{T}_M = -\left(i\nabla + \mathbf{q}_j^I\right)^2, \quad \hat{T}_{\mathrm{GL}} = -\frac{1}{4m}\left(\frac{\hbar}{i}\nabla\right)^2,$$
$$\hat{V}_{\mathrm{GL}}(|\Phi|^2) = (\alpha_s + \beta|\Phi|^2) + \gamma\sum_j|\psi_j|^2, \quad (11)$$

where model parameters $\bar{E}$, $\bar{G}$, $\bar{K}$, $\bar{D}$, $\bar{\gamma}$, and $\bar{M}$ are all rewritten in units of α, while lengths are in units of ξ.

To perform the time evolution, we employ a solution of the form

$$\psi_j(\mathbf{r}, t + \Delta t) = e^{-\Gamma_M\int_t^{t+\Delta t}\hat{F}_M(t)dt}\psi_j(\mathbf{r}, t),$$
$$\Phi(\mathbf{r}, t + \Delta t) = e^{-\Gamma_{\mathrm{GL}}\int_t^{t+\Delta t}\hat{F}_{\mathrm{GL}}(t)dt}\Phi(\mathbf{r}, t) \quad (12)$$

and use the numerical time evolution method known as split-operator technique [15], which consists in splitting the time evolution operator as [24,25]

$$e^{-\Gamma_{M(\mathrm{GL})}\int_t^{t+\Delta t}\hat{F}_{M(\mathrm{GL})}(t)dt} \approx e^{-\frac{i}{2\hbar}\hat{V}_{M(\mathrm{GL})}\Delta_t}e^{-\frac{i}{2\hbar}\hat{T}_{M(\mathrm{GL})}\Delta_t}e^{-\frac{i}{2\hbar}\hat{V}_{M(\mathrm{GL})}\Delta_t} + O(\Delta t^3), \quad (13)$$

where the $O(\Delta t^3)$ error accounts for the noncommutativity between the $\hat{V}_{M(\mathrm{GL})}$ and $\hat{T}_{M(\mathrm{GL})}$ operators. Notice that the $\hat{V}_{M(\mathrm{GL})}$ terms in Eq. (11) depend on $\psi_j(\Phi)$ itself, thus being intrinsically time-dependent, which would require a time integral in the $\hat{V}_{M(\mathrm{GL})}$-dependent terms in Eq. (13). We circumvent this problem by approximating $\hat{V}_{M(\mathrm{GL})}$ to be effectively constant within the time interval $[t, t + \Delta t]$, assuming $\Delta t/\Gamma_{M(\mathrm{GL})}$ small enough to produce a converged energy result with $\lesssim 1\%$ error. As the initial set of order parameters $\psi_j(x, y, t = 0)$ and $\Phi(x, y, t = 0)$ evolve in time, they eventually converge to the order parameter profiles that minimize the McMillan-Ginzburg-Landay energy functional.

Some of the cases we will discuss further require a vector field $\mathbf{q}_j^I(x, y)$ as the incommensurability wave-vector, rather than a constant wave-vector. This may create problems for the practical application of the exponential of the $\hat{T}$ term in Eq. (13), which now includes both derivative operators and functions in the argument of the exponential. This problem is overcome by the use of the gauge-invariant finite difference method proposed in Ref. [26].

III. RESULTS AND DISCUSSION

For the results discussed in this section, we take the choice of parameters $G = K = 2\alpha$, $M = \alpha$, and $D = -\alpha$, the same as in Ref. [9], unless otherwise stated. This allows us to compare our results to previous literature while enabling us to subsequently change the parameters independently and observe how they affect the results. As we will discuss in what follows, the choice $M = -D$ calibrate the relative phases between order parameters such that they produce a CDW with a network of discommensurations that is similar to that experimentally observed for CDW in transition metal dichalcogenides [27]. The choice $G = K$ is also reasonable, as both parameters are linked to energy terms that are quadratic on ψ_j. Nevertheless, we verify that numerical results do not qualitatively depend on this choice. Moreover, while we will

investigate the effect of the CDW profile on the SC phase, we will neglect the influence of the SC order parameter back on the CDW profile. This is a reasonable approximation, since the CDW is already well settled in place when the critical temperature for the superconducting phase is reached. This fact is supported by the phase diagram of several materials, e.g., cuprates and iron-pnictides [18,28–31].

A. Physical insights from a phase-only approximation

In terms of the amplitude and phase of each order parameter, the McMillan energy functional is rewritten as

$$F_{\rm cdw} = \sum_{j=1,2,3} \left\{\tau\phi_j^2 + G\phi_j^4 + \xi^2\left[\left(\mathbf{q}_j^I - \nabla\theta_j\right)^2\phi_j^2 + (\nabla\phi_j)^2\right] - E\phi_j^2\cos(2\theta_j)\right\} - \phi_1\phi_2\phi_3 \times \left[3D\cos(\Theta) + M\sum_{j=1,2,3}\cos(\Theta_j)\right] + \frac{K}{2}\sum_{i\neq j}\phi_i^2\phi_j^2, \tag{14}$$

where $\Theta = \theta_1 + \theta_2 + \theta_3$ and $\Theta_j = \theta_j - \theta_{j+1} - \theta_{j+2}$.

From this functional, it becomes immediately clear that, in a phase-only model, i.e., for constant ϕ_j, in the absence of any coupling term and for $E = 0$, the solution that minimizes the energy has $\nabla\theta_j = \mathbf{q}_j^I$. This suggests that as $E \to 0$, the solution must approach the incommensurate case, for which $\theta_j = \mathbf{q}_j^I \cdot \mathbf{r}$ and, consequently, the phase simply adds a $\mathbf{q}_j^I$ correction to the CDW wave vector $\mathbf{Q}_j^C$. Moreover, this form of the functional also clarifies the role of the M and D in locking relative phases θ_j such that the combination of cosine terms on Θ and Θ_j minimize the energy. Choosing $M = -D$, for instance, leads to a network of discommensurations in the form of a Kagome lattice, such as the one observed for 1T-TaS_2, [27] but other networks can be obtained with different choices of M and D.

The Euler-Lagrange equation for θ_j that minimize $F_{\rm cdw}$ reads

$$\phi_j\nabla^2\theta_j + 2\nabla\phi_j\nabla\theta_j - 2\mathbf{q}_j^I\cdot\nabla\phi_j - \frac{E}{\xi^2}\phi_j\sin(2\theta_j) - \frac{3D}{2\xi^2}\phi_{j+1}\phi_{j+2}\sin(\Theta) - \frac{M}{2\xi^2}\phi_{j+1}\phi_{j+2} \times [\sin(\Theta_j) - \sin(\Theta_{j+1}) - \sin(\Theta_{j+2})] = 0. \tag{15}$$

In this equation, one can verify that the incommensurate phase $\theta_j = \mathbf{q}_j^I \cdot \mathbf{r}$ is still a solution of this equation for $E = 0$ even at a nonconstant ϕ_j and nonzero coupling D, since the term involving the latter is zero, as $\Theta = (\mathbf{q}_1^I + \mathbf{q}_2^I + \mathbf{q}_3^I)\cdot\mathbf{r} = 0$ in this case. However, a nonzero coupling constant M does not guarantee the incommensurate solution as the lowest energy state in the system. Therefore, increasing the coupling constant M may harness the ability to control the transitions between commensurate, discommensurate and incommensurate phases of the CDW only through the parameter E. This strong coupling case will be discussed in more detail in the next Section.

Furthermore, in the phase-only model in the absence of couplings and for nonzero E, Eq. (15) reduces to

$$\nabla^2\theta_j - \frac{E}{\xi^2}\sin(2\theta_j) = 0, \tag{16}$$

which is easily identified as the sine-Gordon equation, whose solution takes the form of a soliton. This suggests that increasing E leads to soliton-like solutions for the phase, which would perfectly mimic the experimentally observed discommensurations in CDW. Since the stationary soliton solution has the general form $\theta_j(x_j) \propto \tan^{-1}\{\exp[\sqrt{E}(x_j - x_{j0})/\xi]\}$, where x_j is the coordinate along the jth direction and x_{j0} is an offset for the soliton position, the sharpness of the soliton steps is controllable by either E or ξ, which are related to the total charge density and the deviation parameter δ_j, respectively.

The analysis of these limits in our model suggests that in the absence of couplings: (i) $E \to 0$ leads to the incommensurate solution, (ii) moderate values of E lead to a combination between an incommensurate phase and soliton-like phase-slips, which can be seen as discommensurations, and (iii) $E \to \infty$ leads to an infinitely long soliton-like step, which is eventually interpreted as the commensurate phase. It is now important to check how the presence of couplings between the different CDW order parameters changes this scenario, which will be done further on in this paper.

The prediction that $\nabla\theta_j$ must converge to $\mathbf{q}_j^I$ to minimize the energy can be used as a convenient way to modify the MGL model as to produce different defects in CDW, beyond the aforementioned discommensurations. For instance, consider a domain wall perpendicular to a given direction $\mathbf{G}_j$, at $x_j = 0$, separating regions where the phase is constant [12,32]. The associated phase θ_j can be mathematically described as a kink function $\theta_j = h_i\tanh(x_j/a_i)$, where a_i and h_i control the width of the interface region and the phase difference across the interface, respectively. Such a phase distribution is readily obtained from the imaginary time evolution by defining an effective incommensurability vector field

$$\mathbf{q}_j^I(x_j) = \frac{h_i}{a_i}\mathrm{sech}^2\left(\frac{x_j}{a_i}\right)\hat{x}_j, \tag{17}$$

such that $\nabla\theta_j = \mathbf{q}_j^I(x)$ yields the expected kink profile for θ_j. As another example of the application of this concept, a vortex-antivortex pair in the CDW along the x axis in θ_j is obtained by an incommensurability vector field [33,34]

$$\mathbf{q}_j^I(x,y) = \left(\frac{-y}{r_v^2} + \frac{y}{r_{av}^2}\right)\hat{x} + \left(\frac{x - \frac{d_{vav}}{2}}{r_v^2} - \frac{x + \frac{d_{vav}}{2}}{r_{av}^2}\right)\hat{y}, \tag{18}$$

where $r_v = \sqrt{(x - d_{vav}/2)^2 + y^2}$, $r_{av} = \sqrt{(x + d_{vav}/2)^2 + y^2}$, and d_{vav} is the vortex-antivortex separation. The profiles of the order parameters obtained from the MGL theory with constant $\mathbf{q}_j^I$, as well as with vector fields defined by Eqs. (17) and (18), are discussed in what follows.

B. Discommensurations revisited

Let us first discuss the case of constant $\mathbf{q}_j^I = \delta_j\mathbf{Q}_j^C$, which leads to discommensurations. For the sake of simplicity, in

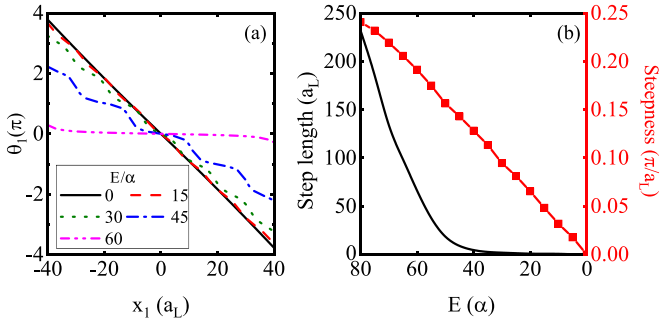

FIG. 1. (a) Phase of the $j = 1$ order parameter along the x_1 direction, assuming different values of lock-in energy $E/\alpha = 0$, 15, 30, 45, and 60. (b) Length of the discommensuration steps (black line, left axis), along with the discommensuration steepness (red line-symbols, right axis), as a function of the lock-in energy E. The lock-in energy axis is reversed to help the visualization, since the actual experimentally controllable parameter is the overall charge density, which is inversely proportional to E.

this Section, we consider the same value δ_j in all three directions ($j = 1 - 3$). Figure 1(a) shows the phase distribution along the reciprocal lattice vector direction $j = 1$, for several values of the energy parameter E, considering $\delta_j = 0.1$. To facilitate the comparison to experiments, lengths are given in units of the lattice parameter $a_L = 2\pi/\mathbf{G}_1$, which can also be retrieved from the characteristic length ξ in previous Sec. II A by $a_L = 2\pi\delta_1\xi$. Results and conclusions for the other directions $j = 2$ and 3 are the same as for 1 and, therefore, are omitted. For $E = 0$, the phase is simply $\theta_1(x_1) = q_1^I x_1$, namely, the system is in a perfectly incommensurate phase, i.e., the effective wave-vector of the CDW in this direction is $Q_1^C(1 + \delta_1) = 1.1Q_1^C$. As E increases, the soliton-like steps predicted in the previous section are observed, thus creating regions where the system is locally commensurate, separated by phase slips, i.e., discommensurations. Eventually, for higher E, the soliton steps are so long that the phase is virtually constant and, therefore, the effective wave-vector of the CDW is simply Q_1^C, thus yielding the commensurate phase. By taking the derivative of θ_1 and computing the height and distance between the resulting peaks, one can estimate the discommensuration steepness and the length of the steps produced by them, respectively. The former (latter) is shown as a red line-squares (black line) in Fig. 1(b) as a function of the lock-in energy E. Since the discommensuration length of the steps can be effectively measured by current experimental techniques, see, e.g., Ref. [12], the results provided here allow one to estimate some of the parameters needed for a proper theoretical description of an actual CDW phase in a given TMD. Increasing the lock-in energy (i.e., decreasing the overall charge density), the discommensuration step length rapidly increases, eventually leading to the commensurate phase.

As mentioned in the previous section, the coupling parameter M is expected to be the most detrimental one for the emergence of discommensurations in the CDW phase profile. The effect of this coupling on the discommensurations, i.e., the dependence of the discommensuration step length and height on M, is shown in Fig. 2. As M increases, the step lengths become shorter, which results in shorter distances

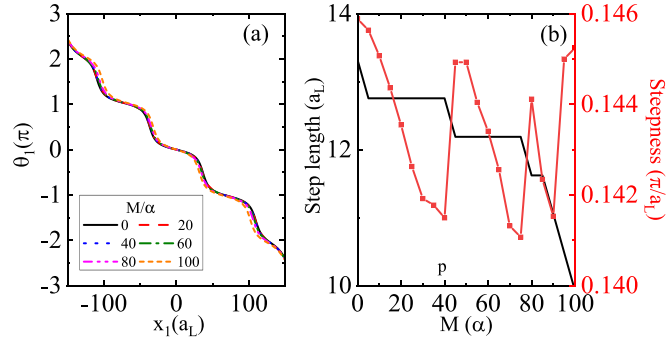

FIG. 2. The same as described in the caption of Fig. 1, but for fixed $E = 50\alpha$, and varied values of the third-order coupling energy $M/\alpha = 0$, 20, 40, 60, 80, and 100.

between the discommensurations, see Fig. 2(a). An approximate 30% decrease in the step length is observed as M increases from zero to 100α. The steepness, however, is not significantly affected by this parameter, since the oscillations in Fig. 2(b), with amplitude less than 3% of the average value, are in the same order of magnitude as the numerical error in our calculations.

The long and steep steps in the phase profiles observed in Fig. 1 become significantly smaller as one increases the incommensurability factor δ_j. This is illustrated in Fig. 3, where we consider $\delta_j = 0.15$. In this case, increasing E within the same range as in Fig. 1, the step length is still two orders of magnitude shorter than that observed in the $\delta_j = 0.1$ case, while the steepness is ≈30% smaller.

Increasing the lock-in energy E effectively increases the critical temperature of the CDW, as inferred by Eq. (15), where one sees that the temperature parameter $\tau = T/T_{\rm cdw} - 1$, which multiplies ϕ_j^2, is effectively changed to $T/T_{\rm cdw} - 1 - E\cos(2\theta_j)$. As E increases and the phase converges to $\theta_j = 0$ as the lowest energy (commensurate) solution, higher temperatures are required to induce the normal-to-CDW phase transition. However, how fast θ_j converges to zero depends on the different system parameters: higher discommensuration factors δ_j, for example, lead to a delayed convergence of θ_j to zero at significantly higher E. Therefore, the control of the CDW critical temperature is expected to depend, e.g., on δ_j, which is confirmed by our numerical results in Fig. 4, which shows the effective critical temperature as a function of the lock-in energy E for different values of δ_j. The delayed

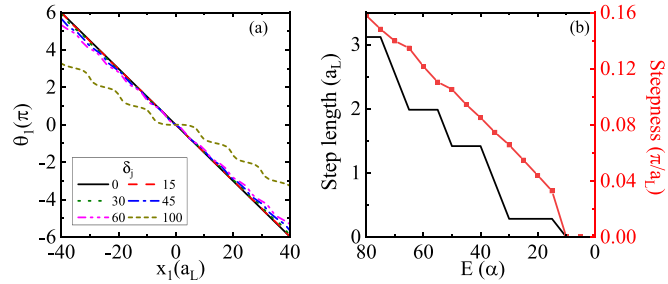

FIG. 3. Same as described in the caption of Fig. 1, but for $\delta_j = 0.15$. Notice that, in this case, a higher value of the lock-in energy is needed to achieve the soliton solution.

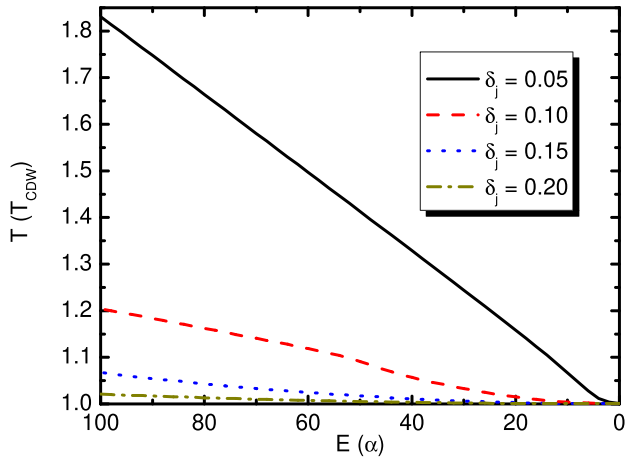

FIG. 4. Effective critical temperature as a function of the lock-in energy E for different values of the discommensuration parameter δ_j, taken the same for all three reciprocal vector directions $j = 1 - 3$.

convergence of $\cos(2\theta_j)$ to 1 for higher δ_j eventually hinders the contribution of E to the effective critical temperature, thus making the control of the CDW critical temperature via E less efficient.

C. Phase domain walls and topological defects

Figures 5(a) and 5(b) show color maps of CDW profiles, calculated with Eq. (1), in the presence of a phase domain wall. Such domain walls are obtained by defining the incommensurability vector fields $\mathbf{q}_1^l(x, y)$ and $\mathbf{q}_2^l(x, y)$ as in Eq. (17),

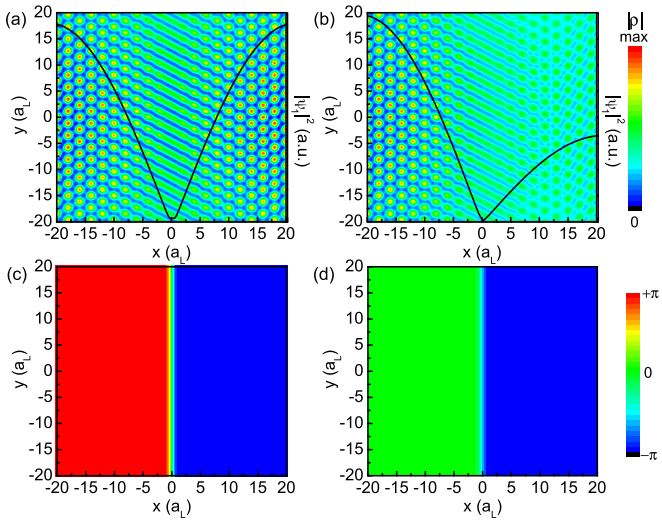

FIG. 5. (a), (b) Color maps of the CDW profile in the presence of a phase domain wall in the order parameters ψ_1 and ψ_2, obtained by defining their incommensurability vector fields as in Eq. (17). The amplitude of the order parameter ψ_1 along the x direction (solid curve) is superposed on the color map, for comparison. The amplitude of the order parameter ψ_2 is the same in this case. Two types of domain walls are obtained from the calculations: (a) one with a 2π-phase slip and (b) the other with a π-phase slip. The corresponding phase distributions of the CDW order parameter ψ_1 in each of these cases are shown in panels (c) and (d), respectively.

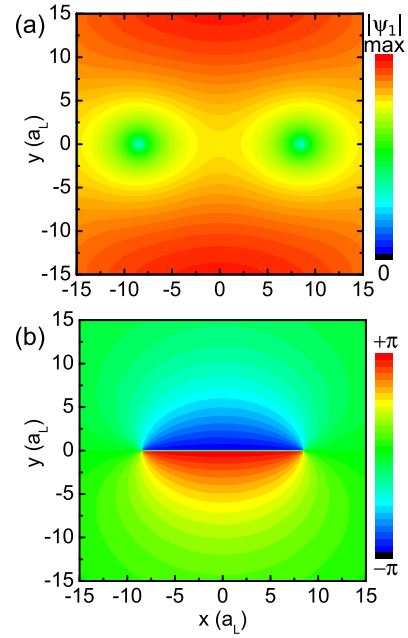

FIG. 6. (a) Amplitude and (b) phase of the CDW order parameter ψ_1, obtained by defining the incommensurability vector field as in Eq. (18).

which leads to the formation of identical domain walls in the order parameters ψ_1 and ψ_2, as observed in Ref. [12]. Indeed, the phase slips observed due to these domain walls in Figs. 5(c) and 5(d) lead to a CDW profile that qualitatively resembles those experimentally observed, e.g., in Refs. [12,32]. The amplitude (squared modulus) of the ψ_1 order parameter is shown as a solid line in Figs. 5(a) and 5(b) and exhibits a strong suppression at the interface. The $|\psi_2|^2$ profile is the same, and is therefore not shown.

Results in Figs. 5 and 6 were obtained considering $E = 40\alpha$, but we have verified that changing the value of E from 0 to 100 α does not affect these profiles. Either in the presence of a domain wall or the vortex-antivortex pair topological defect, it is clear that along the line where the phase of the CDW order parameter changes abruptly, its amplitude locally drops to low values, thus enabling the emergence of a SC phase, as we will discuss later.

Starting the imaginary time evolution with random initial functions ψ_j, the 2π-phase slip domain wall shown in Figs. 5(a) and 5(c) is readily obtained. However, experiments in Ref. [12] actually reveal a π-phase slip, such as the one shown in Figs. 5(b) and 5(d), which is obtained by our model as a solution with slightly larger energy as compared to the 2π-phase slip case. It is thus regarded as a metastable state of the McMillan energy functional presented here, obtained with an appropriate choice of initial function that already exhibits such a phase-slip and is then properly converged through the imaginary time evolution procedure. From Fig. 5(b), one also observes that the amplitude of the order parameter with a π-phase slip is different on two sides of the domain wall, which leads to different amplitudes of the CDW on each side as well. A full sweep of the parametric space within the McMillan model presented here, to produce a phase diagram

and eventually search for a situation where π-phase slips are energetically favored is outside the scope of the present work and is left as a future perspective of this study.

Figure 6 illustrates the phase and amplitude obtained from our calculations defining the incommensurability vector field $\mathbf{q}_1^I(x, y)$ as in Eq. (18), which yields the formation of a vortex-antivortex pair, assuming a separation $d_{vav} = 60\,\xi$. As expected, the CDW amplitude strongly drops in the cores of the vortex and the antivortex, with a line of suppressed CDW amplitude connecting them, in qualitative agreement with the experimental observations in Ref. [12].

D. CDW with broken rotational symmetry

Recent experiments on $NbSe_2$ have also observed a CDW phase consisting of a wave with a single direction, for example $\mathbf{Q}_3^C > 0$, while the effective wave vector is zero for the remaining directions, which constitutes the so called unidirectional charge density wave phase (1q-CDW) [12]. In the model proposed here, a qualitatively similar phase can be achieved by considering an anisotropic form for the incommensurability vectors $\mathbf{q}_j^I = \delta_j \mathbf{Q}_j^C$, such that two of the discommensuration parameters are equal to 1, e.g., $\delta_1 = \delta_2 = 1$, while δ_3 may assume a small value, which we will set to $\delta_3 = 0.1$ here as an example. We have verified that a numerical solution of Eq. (7) with this set of values for δ_j is unstable if the terms that couple different order parameters in the first order, namely those proportional to D and M, are nonzero. However, such one-directional phase is in fact experimentally observed, suggesting a way to possibly rule out some coupling terms that, although allowed by symmetry [9], may be negligible in some physical situations. Therefore, results in this section are discussed assuming $D = M = 0$.

Figure 7 shows the CDW profile with this set of parameters, which indeed leads to unidirectional CDW along the Q_3^C direction. In the case of zero lock-in energy $E = 0$, no defect is observed in the CDW periodicity; see Fig. 7(a). A perfectly periodic, although incommensurate, CDW profile is obtained in this case. However, as the lock-in energy is increased to $E = 40\alpha$, our model predicts the occurrence of phase slips in the CDW profile, due to discommensurations; see Fig. 7(b). Such discommensurations in the 1q-CDW predicted here for intermediate values of E are yet to be experimentally verified. For the $E = 100\alpha$ case in Fig. 7(c), we obtain a commensurate unidirectional CDW with no defects. Figure 7(d) shows the profile of a cross section of the CDW along the direction perpendicular to the wave fronts, for the $E = 0$ (black solid line) and $E = 100\alpha$ (red dashed line) cases, to emphasize the difference between the results shown in Figs. 7(a) and 7(c). One verifies that the former, which is incommensurate, has a wavelength 10% smaller than the latter, due to our choice of the discommensuration parameter $\delta_3 = 0.1$. It is easy to infer that unidirectional CDW in the $j = 1, 2$ directions can be similarly obtained simply by making $\delta_j \neq 0$ and $\delta_n = 1$ for $n \neq j$.

Notice that the minima in the 1q-CDW profile $\rho(\mathbf{r})$ shown in Fig. 7 for $E = 0$ and $E = 100\alpha$ do not result from a modulation of the amplitude of the order parameter, but rather from the oscillations originating from the exponential terms in Eq. (1). Therefore, the minima in these 1q-CDW cases are not expected to affect the SC phase, which couples to the order parameters ψ_j, rather than to the total CDW density profile ρ in the MGL model. Conversely, the amplitude modulation resulting from the discommensurations in Fig. 7(b) for $E = 40\alpha$ is expected to lead to significant effects on SC.

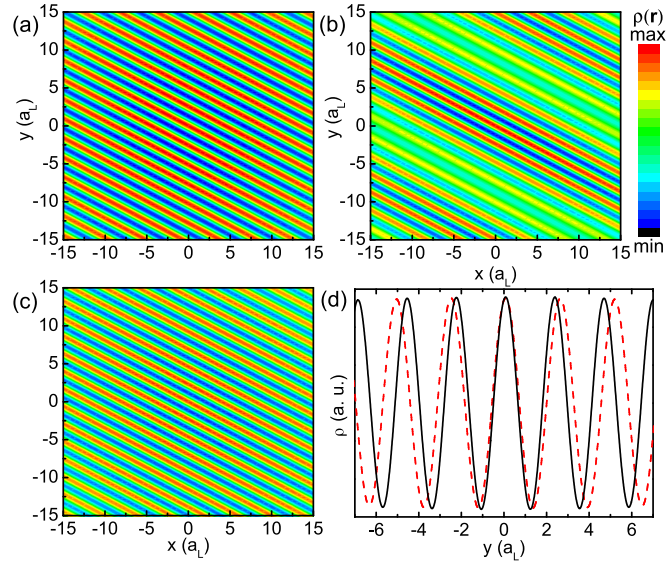

FIG. 7. CDW distribution $\rho(\mathbf{r})$ assuming an anisotropic set of incommensurability vectors, such that $\mathbf{q}_3^I = 0.1\mathbf{Q}_3^C$, $\mathbf{q}_2^I = \mathbf{Q}_2^C$, and $\mathbf{q}_1^I = \mathbf{Q}_1^C$, for $D = M = 0$, thus leading to an unidirectional charge density oscillation. Three values of lock-in energy are considered: (a) $E = 0\alpha$, (b) $E = 40\alpha$, and (c) $E = 100\alpha$. (d) Cross section of the CDW profiles for $E = 0\alpha$ (black solid line) and $E = 100\alpha$ (red dashed line) along the y-direction at $x = 0$, emphasizing the 10% smaller wavelength in the former, as a result of the $\delta_3 = 0.1$ discommensuration parameter.

E. Effects on the emergent superconducting phase

Finally, we discuss qualitatively the effect on superconductivity of the CDW defects discussed in the previous sections. As previously mentioned, our model simulates a superconducting order parameter Φ competing with the CDW order parameters ψ_j, which are coupled via the parameter γ in Eq. (2). The superconducting phase is expected to emerge in the regions of space where the CDW order parameters are suppressed, due to competition that is closely related to the hidden order parameter model discussed in Refs. [13,14]. In fact, the equivalence between the bi-quadratic coupling considered in Eq. (2) and the coupling proposed in Ref. [9] can be seen by collecting all terms that multiply $|\psi_j|^2$ in the former into an effective $\alpha_s^* = \alpha_s + \sum_j \gamma |\psi_j|^2$. Assuming the usual temperature dependence in GL theory [35], namely, $\alpha_s(T) = \alpha_0(T/T_{SC} - 1)$, where T_{SC} is the reference value of the superconducting critical temperature and α_0 defines the SC coherence length at $T = 0$K, the γ coupling effectively reduces the critical temperature of the superconducting phase locally wherever the amplitude of the CDW order parameter $|\psi_j|^2$ is high. From here onward, temperatures are rescaled to T_{SC} for clarity, i.e., in the absence of CDW, the SC phase transition would occur at $T/T_{SC} = 1$, and distributed $|\psi_j|^2$

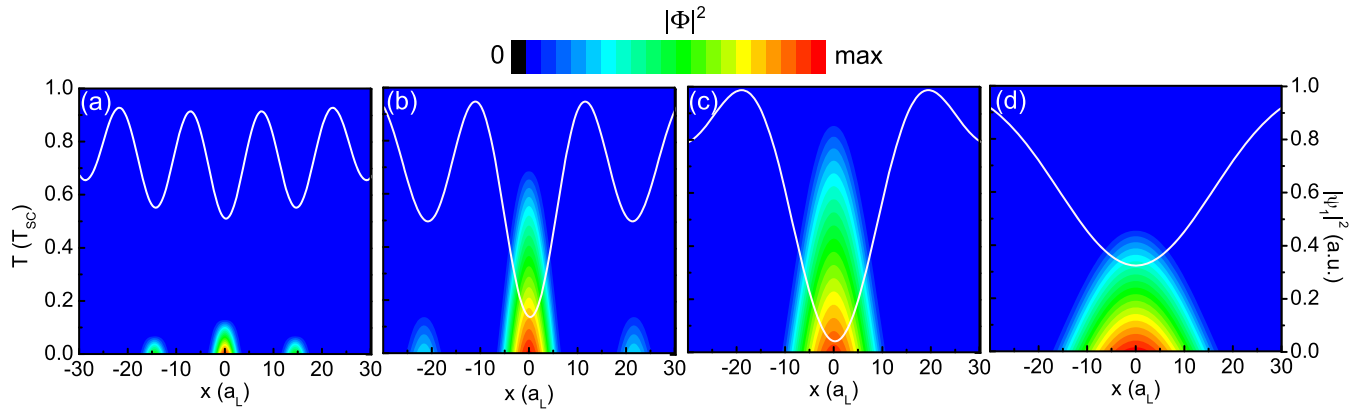

FIG. 8. Color map of the superconducting (Cooper-pair) density below the SC critical temperature T_{SC}, in the system where the CDW order parameter ψ_1 exhibits discommensurations along the x direction, for lock-in energies E equal (a) 40α, (b) 50α, (c) 60α, and (d) 70α, assuming a coupling parameter $\gamma = 4$. The profile of the CDW is superposed in each panel as a solid curve and referred to the right axis of panel (d). The maximum value in each color map is different, to facilitate visualization: $0.2|\phi_0|^2$ (a), $0.8|\phi_0|^2$ (b), $1|\phi_0|^2$ (c), and $0.5|\phi_0|^2$ (d), where $|\phi_0|^2$ is the SC density in absence of any CDW.

will accordingly suppress superconductivity and consequently reduce the effective SC critical temperature.

In what follows, for the sake of simplicity, we will discuss the rise of the superconducting order parameter in the interstitial spaces of a 1D-CDW found in the previous section. This approximation allows us to conveniently qualitatively predict the behavior of the superconducting critical temperature dome in terms of the parameters of the CDW. A generalization of this discussion to the case of a combination of three CDW order parameters is then straightforward. The GL equation for the SC order parameter resulting from this approximation reads [13]

$$-\frac{1}{\xi_r^2}\frac{d^2\Phi}{dx^2} + \left[\frac{T}{T_{SC}} - \left(1 - \frac{\gamma}{\xi_r^2}|\psi_1|^2\right) + |\Phi|^2\right]\Phi = 0, \quad (19)$$

where we assume a ratio of coherence lengths of CDW and SC order parameters as $\xi_r = \xi/\xi_{SC} = 0.7$, as an illustrative example.

The amplitude of the CDW order parameter exhibits dips at the discommensurations, whose depth is given by the steepness of the discommensuration. Within the model employed here, the effective superconducting critical temperature increases as the dips in the CDW are deeper and closer to each other [13]. Therefore, Fig. 1 allows us to predict that, for low values of E, the discommensurations become steeper as E increases, thus increasing the superconducting critical temperature. However, for intermediate E, the discommensurations separate further from each other, decreasing the critical temperature again, until the commensurate phase is reached, where discommensurations are no longer seen. This qualitatively explains the emergence of a superconducting dome in the temperature versus charge density phase diagram. Indeed, this behavior is verified in the color maps of the calculated SC order parameter along the x axis as a function of temperature in Fig. 8. The profile of the CDW order parameter for E equal 40α, 50α, 60α, and 70α are shown as a white solid curve in Figs. 8(a)–8(d), respectively, for comparison. For $E = 60\alpha$, the dips in this order parameter are deep and close, leading to a nonzero SC order parameter almost up to $T = T_{SC}$ for $\gamma = 4$, cf. Fig. 8(c). However, superconductivity in the center of the sample vanishes at lower effective critical temperatures as E is made either higher or lower than $E = 60\alpha$. For either $E < 40\alpha$ or $E > 90\alpha$, these dips are no longer able to sustain superconductivity and the effective SC critical temperature drops to zero.

Figure 9 shows the SC dome delimited by the effective critical temperatures found as the temperature at which $|\Phi|^2$ drops to zero for each value of E. In the case where the discommensuration parameter is $\delta_1 = 0.10$ and the coupling between SC and CDW order parameters is strong, the SC dome reaches values as high as 85% of the nominal SC critical temperature at $E = 40\alpha$, for $\gamma = 2.5$. Considering a lower coupling parameter, $\gamma = 2.0$, the SC dome becomes smaller. It is challenging to relate the strength of the SC-CDW coupling in the phenomenological model proposed here to an actual material sample, but the behavior of the SC dome for systems with different discommensuration lengths can be compared. In this case, our model predicts that for $\delta_1 = 0.12$,

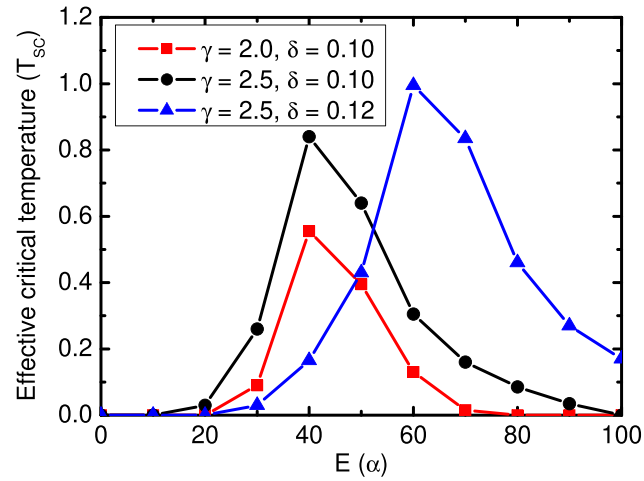

FIG. 9. Superconducting dome, delimited by the effective SC critical temperature as a function of the lock-in energy, assuming $\gamma = 2.0$ (red) and 2.5 (black) for a $\delta_1 = 0.1$ discommensuration parameter, and $\gamma = 2.5$ for $\delta_1 = 0.12$ (blue).

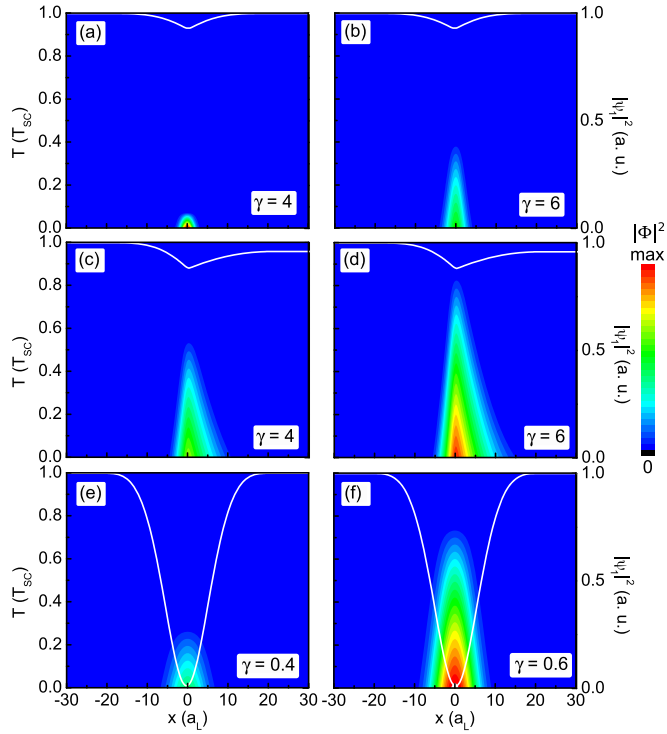

FIG. 10. Color map of the SC Cooper-pair density in the region of suppressed CDW order as the temperature T decreases below the SC critical temperature T_{SC}. We consider CDW order parameter ψ_1 that is suppressed either due to [(a), (b)] a 2π-phase domain wall, [(c), (d)] a π-phase domain wall, or (e, f) a vortex-antivortex defect along the x direction. Two values of the coupling parameter γ between SC and CDW are considered in each case, as shown by the labels in each panel. The profile of the amplitude of the CDW order parameter ψ_1 along the x direction is shown in each panel as a white line, for comparison. The maximum value in each color map is different, to facilitate visualization: $0.1|\phi_0|^2$ (a), $0.9|\phi_0|^2$ (b), $1|\phi_0|^2$ [(c), (d)], and $0.9|\phi_0|^2$ [(e), (f)], where $|\phi_0|^2$ is the SC density in absence of any CDW.

where discommensurations are shorter in space and more weakly affected by the lock-in E (cf. Fig. 3), the SC dome becomes considerably higher and wider, as shown by the blue symbols in Fig. 9. Since superconductivity is expected to emerge only at discommensurations, superconducting regions would be further apart also in systems with high coupling M, as suggested by Fig. 2. Consequently, the superconducting dome is expected to exhibit lower critical temperatures in systems with high M as well.

Superconductivity is also expected to emerge within the dips in the CDW order parameter ψ_1 due to domain walls [36] illustrated in Fig. 5, or to the defects illustrated in Fig. 6. Fig. 10 shows a color map of the SC order parameter profile in Figs. 10(a)–10(d) domain wall and Figs. 10(e) and 10(f) vortex-antivortex defects, as a function of temperature T. As in the case where SC rises within discommensurations, a higher γ coupling [Figs. 10(b), 10(d), and 10(f)] also enhances the effective SC critical temperature here, as compared to the cases where γ is lower [Figs. 10(a), 10(c), and 10(e)]. However, for both domain wall and vortex-antivortex defects, changing the lock-in energy E does not significantly affect either the depth or the width of the minimum in ψ_1, as previously discussed in Sec. III C. Therefore, although these defects are expected to enable the emergence of superconductivity in the sample, they are not expected to affect the profile of the SC dome in the temperature versus charge density (or, equivalently, lock-in energy E) phase diagram. Nevertheless, a significant difference is observed in the dip of the CDW order parameter in each case investigated here: when plotted in the same scale, the dip in $|\psi_1|^2$ observed for the 2π-phase domain wall is shallower than the one for the π-phase domain wall, and they both are one order of magnitude shallower than the one observed for the vortex-antivortex pair, as one verifies by comparing the white lines in Fig. 10. As a consequence, the effective SC critical temperature for $\gamma = 4$ in the 2π-phase domain wall case, i.e., Fig. 10(a), is much lower than the one in the π-phase domain wall case for the same γ, as seen in Fig. 10(c). Also, in the vortex-antivortex case, Figs. 10(e) and 10(f) show that one order of magnitude lower γ values lead to similar enhancement of the effective SC critical temperature as in the domain wall defect cases, owing to significantly deeper CDW suppression in that case.

IV. CONCLUSIONS

We have demonstrated how parameters and functional forms of the McMillan-Ginzburg-Landau energy functional for transition metal dichalcogenides are linked to the formation of discommensurations in the CDW phase profiles, the emergence of topological defects (vortex-antivortex pairs) and domain walls in the phase, as well as the appearance of an unidirectional CDW state. We also investigated how modifications of the phase features associated with each of those states affect the resulting profile of the CDW order parameters. With such an analysis, albeit within the phenomenological model, we revealed the mechanism behind the formation of these states, which have been observed in recent experiments. Since CDW order parameter is known to typically compete with an emergent SC order parameter in these systems, we have also used our model to elucidate the emergence of the SC dome in the phase diagram of such materials, and we demonstrated how the SC critical temperature depends on the distance and depth of the modulations in the CDW order parameter. Our model and presented results will therefore help further design of material systems where the interaction of competing collective phenomena is practically tailored at will.

ACKNOWLEDGMENTS

This work was financially supported by the Brazilian Council for Research (CNPq), under the PQ (312705/2022-0), UNIVERSAL (423423/2021-5), and PRONEX/FUNCAP programs, by the Brazilian Council for Higher Education (CAPES), by the Research Foundation Flanders (FWO-Vl), and by the EU-COST Action CA21144 SUPERQUMAP.

[1] D. Chowdhury, E. Berg, and S. Sachdev, Nematic order in the vicinity of a vortex in superconducting FeSe, Phys. Rev. B **84**, 205113 (2011).

[2] E. Fradkin, S. A. Kivelson, M. J. Lawler, J. P. Eisenstein, and A. P. Mackenzie, Nematic Fermi fluids in condensed matter physics, Annu. Rev. Condens. Matter Phys. **1**, 153 (2010).

[3] R. M. Fernandes, A. V. Chubukov, and J. Schmalian, What drives nematic order in iron-based superconductors? Nat. Phys. **10**, 97 (2014).

[4] R. M. Fernandes and J. Schmalian, Competing order and nature of the pairing state in the iron pnictides, Phys. Rev. B **82**, 014521 (2010).

[5] A. B. Vorontsov, M. G. Vavilov, and A. V. Chubukov, Interplay between magnetism and superconductivity in the iron pnictides, Phys. Rev. B **79**, 060508(R) (2009).

[6] W. Shi, J. Ye, Y. Zhang, R. Suzuki, M. Yoshida, J. Miyazaki, N. Inoue, Y. Saito, and Y. Iwasa, Superconductivity series in transition metal dichalcogenides by ionic gating, Sci. Rep. **5**, 12534 (2015).

[7] B. Keimer, S. A. Kivelson, M. R. Norman, S. Uchida, and J. Zaanen, From quantum matter to high-temperature superconductivity in copper oxides, Nature (London) **518**, 179 (2015).

[8] L. J. Li, E. C. T. O'Farrell, K. P. Loh, G. Eda, B. Özyilmaz, and A. H. Castro Neto, Controlling many-body states by the electric-field effect in a two-dimensional material, Nature (London) **529**, 185 (2016).

[9] C. Chen, L. Su, A. H. Castro-Neto, and V. M. Pereira, Discommensuration-driven superconductivity in the charge density wave phases of transition-metal dichalcogenides, Phys. Rev. B **99**, 121108(R) (2019).

[10] W. L. McMillan, Theory of discommensurations and the commensurate-incommensurate charge-density-wave phase transition, Phys. Rev. B **14**, 1496 (1976).

[11] C. S. Lian, C. Si, and W. Duan, Unveiling charge-density wave, superconductivity, and their competitive nature in two-dimensional $NbSe_2$, Nano Lett. **18**, 2924 (2018).

[12] Á. Pásztor, A. Scarfato, M. Spera, C. Barreteau, E. Giannini, and C. Renner, Holographic imaging of the complex charge density wave order parameter, Phys. Rev. Res. **1**, 033114 (2019).

[13] V. N. Moura, D. S. Dantas, G. A. Farias, A. Chaves, and M. V. Milošević, Latent superconductivity at parallel interfaces in a superlattice dominated by another collective quantum phase, Phys. Rev. B **106**, 014516 (2022).

[14] A. Moor, A. F. Volkov, and K. B. Efetov, Hidden order as a source of interface superconductivity, Phys. Rev. B **91**, 064511 (2015).

[15] A. Chaves, G. A. Farias, F. M. Peeters, and R. Ferreira, The split-operator technique for the study of spinorial wavepacket dynamics, Commun. Comput. Phys. **17**, 850 (2015).

[16] A. Achari, J. Bekaert, V. Sreepal, A. Orekhov, P. Kumaravadivel, M. Kim, N. Gauquelin, P. B. Pillai, J. Verbeeck, F. M. Peeters, A. K. Geim, M. V. Milošević, and R. R. Nair, Alternating superconducting and charge density wave monolayers within bulk 6R-TaS_2, Nano Lett. **22**, 6268 (2022).

[17] Y. Nakata, K. Sugawara, A. Chainani, H. Oka, Ch. Bao, Sh. Zhou, P.-Yu Chuang, Ch.-M. Cheng, T. Kawakami, Y. Saruta, T. Fukumura, Sh. Zhou, T. Takahashi, and T. Sato, Robust charge-density wave strengthened by electron correlations in monolayer 1T-$TaSe_2$ and 1T-$NbSe_2$, Nat. Commun. **12**, 5873 (2021).

[18] Y. I. Joe, X. M. Chen, P. Ghaemi, K. D. Finkelstein, G. A. de la Peña, Y. Gan, J. C. T. Lee, S. Yuan, J. Geck, G. J. MacDougall, T. C. Chiang, S. L. Cooper, E. Fradkin, and P. Abbamonte, Emergence of charge density wave domain walls above the superconducting dome in 1T-$TiSe_2$, Nat. Phys. **10**, 421 (2014).

[19] A. E. Jacobs and M. B. Walker, Phenomenological theory of charge-density-wave states in trigonal-prismatic, transition-metal dichalcogenides, Phys. Rev. B **21**, 4132 (1980).

[20] R. K. Kumar, L. E. Young, D. Vudragović, A. Balaž, P. Muruganandam, and S. K. Adhikari, Fortran and C programs for the time-dependent dipolar Gross-Pitaevskii equation in an anisotropic trap, Comput. Phys. Commun. **195**, 117 (2015).

[21] N. G. Parker, C. Ticknor, A. M. Martin, and D. H. J. O'Dell, Structure formation during the collapse of a dipolar atomic Bose-Einstein condensate, Phys. Rev. A **79**, 013617 (2009).

[22] C. Ticknor, N. G. Parker, A. Melatos, S. L. Cornish, D. H. J. O'Dell, and A. M. Martin, Collapse times of dipolar Bose-Einstein condensate, Phys. Rev. A **78**, 061607(R) (2008).

[23] M. Matuszewski, T. Taylor, and A. V. Kavokin, Exciton supersolidity in hybrid Bose-Fermi systems, Phys. Rev. Lett. **108**, 060401 (2012).

[24] F. Trotter, On the product of semi-groups of operators, Proc. Am. Math. Soc. **10**, 545 (1959).

[25] M. Suzuki, Generalized Trotter's formula and systematic approximants of exponential operators and inner derivations with applications to many-body problems, Commun. Math. Phys. **51**, 183 (1976).

[26] M. Governale and C. Ungarelli, Gauge-invariant grid discretization of the Schrödinger equation, Phys. Rev. B **58**, 7816 (1998).

[27] A. W. Tsen, R. Hovden, D. Wang, Y. D. Kim, J. Okamoto, K. A. Spoth, Y. Liu, W. Lu, Y. Sun, J. C. Hone, and L. F. Kourkoutis, Structure and control of charge density waves in two-dimensional 1T-TaS_2, Proc. Natl. Acad. Sci. USA **112**, 15054 (2015).

[28] F. H. Yu, D. H. Ma, W. Z. Zhuo, S. Q. Liu, X. K. Wen, B. Lei, J. J. Ying, and X. H. Chen, Unusual competition of superconductivity and charge-density-wave state in a compressed topological kagome metal, Nat. Commun. **12**, 3645 (2021).

[29] E. Morosan, H. W. Zandbergen, B. S. Dennis, J. W. G. Bos, Y. Onose, T. Klimczuk, A. P. Ramirez, N. P. Ong, and R. J. Cava, Superconductivity in Cu_xTiSe_2, Nat. Phys. **2**, 544 (2006).

[30] A. F. Kusmartseva, B. Sipos, H. Berger, L. Forró, and E. Tutiš, Pressure induced superconductivity in pristine 1T-$TiSe_2$, Phys. Rev. Lett. **103**, 236401 (2009).

[31] A. Kogar, G. A. de la Pena, S. Lee, Y. Fang, S. X.-L. Sun, D. B. Lioi, G. Karapetrov, K. D. Finkelstein, J. P. C. Ruff, P. Abbamonte, and S. Rosenkranz, Observation of a charge density wave incommensuration near the superconducting dome in Cu_xTiSe_2, Phys. Rev. Lett. **118**, 027002 (2017).

[32] Sh. Yan, D. Iaia, E. Morosan, E. Fradkin, P. Abbamonte, and V. Madhavan, Influence of domain walls in the incommensurate charge density wave state of Cu intercalated 1T-$TiSe_2$, Phys. Rev. Lett. **118**, 106405 (2017).

[33] A. Chaves, F. M. Peeters, G. A. Farias, and M. V. Milošević, Vortex-vortex interaction in bulk superconductors: Ginzburg-Landau theory, Phys. Rev. B **83**, 054516 (2011).

[34] A. Chaves, L. Komendová, M. V. Milošević, J. S. Andrade, Jr., G. A. Farias, and F. M. Peeters, Conditions for nonmonotonic vortex interaction in two-band superconductors, Phys. Rev. B **83**, 214523 (2011).

[35] M. V. Milošević and R. Geurts, The Ginzburg-Landau theory in application, Physica C: Superconductivity **470**, 791 (2010).

[36] S. Lee, J. Collini, S. X.-L. Sun, M. Mitrano, X. Guo, C. Eckberg, J. Paglione, E. Fradkin, and P. Abbamonte, Multiple charge density waves and superconductivity nucleation at antiphase domain walls in the nematic pnictide $Ba_{1-x}Sr_xNi_2As_2$, Phys. Rev. Lett. **127**, 027602 (2021).